Infrared Signatures of Proton Transfer in Guanine·Cytosine and Adenine·Thymine Base Pairs: DFT Study

TOMOYUKI HAYASHI AND SHAUL MUKAMEL*
Department of Chemistry, University of California, Irvine, Irvine, California 92697, USA

(Received 25 September 2003 and in revised form 10 October 2003)

Abstract. The structures of all stable tautomers of guanine·cytosine and adenine·thymine Watson–Crick base pairs produced by single and double proton transfers from the most stable structures are optimized using density functional theory (DFT) at the B3LYP/6-31G(d,p) level. The zwitterionic tautomer of guanine·cyosine is stable in a high-dielectric medium (water), but not in the gas phase. Normal mode calculations show that the infrared peak positions and intensities of the carbonyl, N–H, and O–H stretching modes are sensitive to the tautomer geometries.

1. INTRODUCTION

Antiparallel amino N–H···O=C and amide N–H···N hydrogen bonds occurring in the adenine·thymine (A·T) and guanine·cytosine (G·C) base pairs (Fig. 1) in the DNA double helix play key roles in genetic molecular recognition and structure determination of nucleic acid base pairs.[1,2] The rare imino/enol tautomers of Watson–Crick G·C and A·T base pairs formed during DNA unwinding and strand separation are thought to be responsible for the formation of spontaneous substitution mutation.[3,4] The energy differences of these tautomers affect proton transfer dynamics[5–7] and are crucial for genetic instabilities. Hydrogen bonding can also affect charge transfer in DNA.[8]

Several G·C tautomers were located and their energies were computed by Florian and Leszczynski[4] by geometry optimizations at the restricted Hartree–Fock (RHF/6-31G(d)) level, including the solvent through the self-consistent reaction field (SCRF) method. However, the single point energies of these optimized structures computed at a higher level MP2/6-31G(d,p) gave different relative energies, indicating that electron correlations are important for reliable energy and geometry optimizations.

The dynamics of the double proton transfer in model DNA compounds has been extensively studied experimentally and theoretically.[9–14] The concerted mechanism was proposed for the 7-azaindole dimer,[10,11] and the stepwise mechanism was proposed for the 2-aminopyridine/acetic acid system.[14]

Infrared spectra of base pairs and DNA molecules have been reported by Tsuboi, M.[15,16] The IR of poly dG·poly dC and poly dA·poly dT in D_2O were compared to the corresponding single strands, and the spectral changes observed in the 1500–1700 cm^{-1} region were attributed to the formation of base pairs. The infrared spectra of dA·dT in D_2O at increasing temperatures from 278 K to 343 K also showed the continuous spectral changes in the same region, reflecting the hydrogen-bond breaking and disruption of the Watson–Crick base pairs.

In the present study we carried out geometry optimization of all possible G·C and A·T tautomers produced by single and double proton transfers from the most stable structures using density functional theory (DFT) at the B3LYP/6-31G(d,p) level. Normal mode calculations were performed for optimized tautomers to identify the infrared features which are most sensitive to geometry. The peaks of each tautomer cannot be resolved by linear infrared spectroscopy at room temperature because the population mostly resides in the most stable tautomer. However, our previous study[17,18] had demonstrated that three pulse nonlinear infrared

*Author to whom correspondence should be addressed. E-mail: smukamel@uci.edu

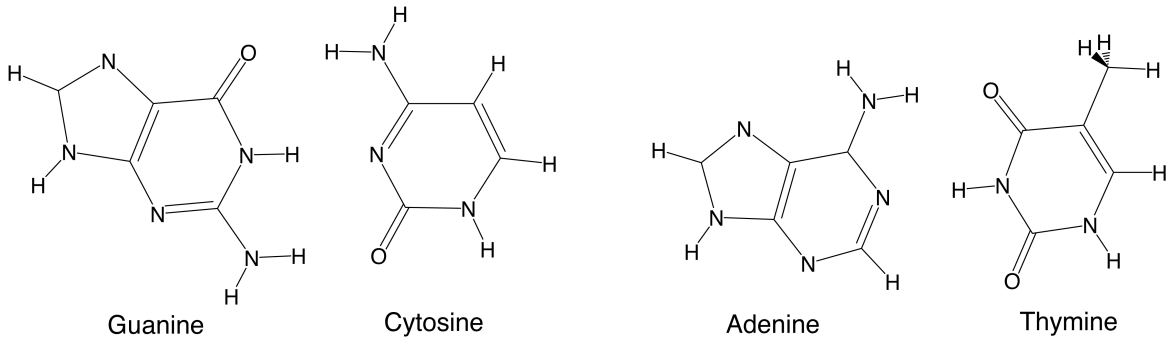

Fig. 1. Watson–Crick guanine·cytosine (G·C) and adenine·thymine (A·T) base pairs.

spectra[19–24] of proton transfer systems are very sensitive to the global potential energy surface (PES) along the proton transfer coordinate. The spectra of the various species can therefore be studied with nonlinear infrared techniques.

The present study of the optimization and normal mode calculation of several tautomers of Watson–Crick G·C and A·T base pairs should form the basis for the simulation of the nonlinear infrared spectra of DNA. The first such experimental study was reported recently.[25]

2. STABLE TAUTOMERS OF BASE PAIRS

2.1 G·C Base Pair

Geometry optimizations of the three tautomers which were found most stable and proposed to be involved in the proton transfer by Florian[4] were carried out by density functional theory. All geometry optimizations and normal mode calculations were carried out at the B3LYP/6-31G(d,p) level using GAUSSIAN 98,[26] where *p*-type polarization functions were only added on H atoms involved in the hydrogen bondings. Solvent effects were taken into account by the SCRF method[27–31] using the dielectric constant of water ε_r = 78.39. We obtained the cavity radius a_0 = 4.87 Å of the most stable Watson–Crick tautomer (GC0) (Fig. 2) self-consistently related to the same permittivity by the molecular volume calculation, and used it for all tautomers. C_s symmetry was assumed in all calculations. Three energy minima, GC0, GC1, and GC2 (Fig. 2), were found. GC1 is a zwitterionic tautomer formed from GC0 by a single proton transfer (PT1). GC2 is a second stable tautomer

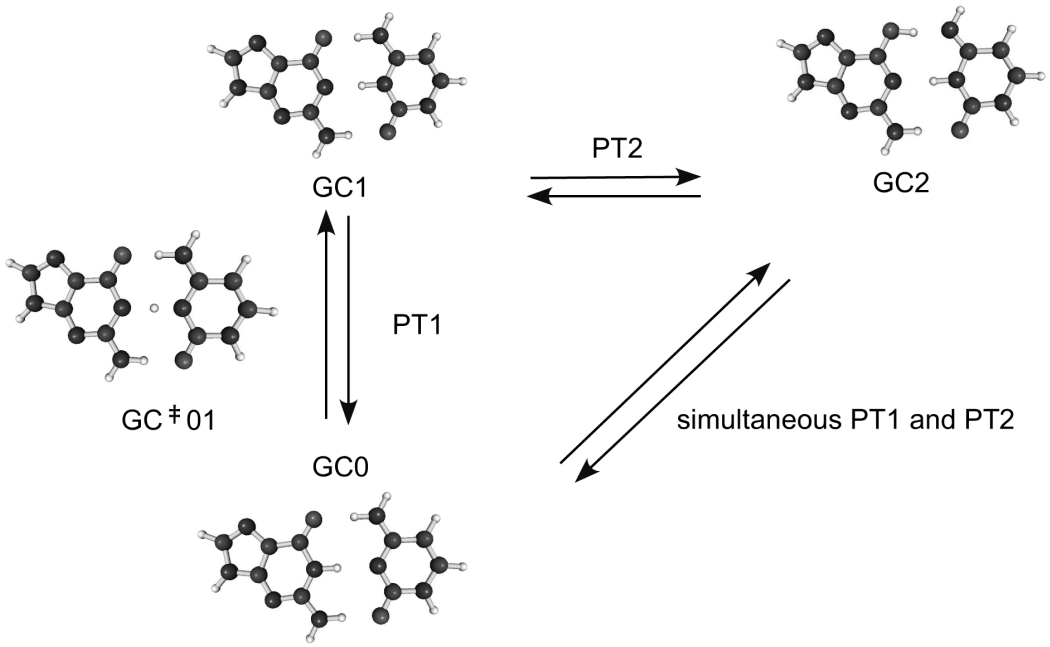

Fig. 2. Located energy minima of guanine·cytosine base pair. Geometry optimizations were carried out at the B3LYP/6-31G(d,p) level with SCRF method assuming the cavity radius of 4.87 Å and the dielectric constant of 78.39 (water).

which can be formed either from GC1 via a second proton transfer (PT2) or from GC0 via a simultaneous double proton transfer (simultaneous PT1+PT2). GC‡01 is the transition state between GC0 and GC1. Other transition states between GC0 and GC2, GC1, and GC2 could not be located. The relative energies of these configurations are shown along with the gas phase calculations and compared with the RHF/6-31G(d)/SCRF study[4] in Table 1. Calculated hydrogen bond geometries of all tautomers are reported in Table 2.

We notice some important differences between SCRF and gas phase calculations. The zwitterionic GC1 tautomer could not be located in the gas phase calculation. There are also significant differences between DFT and RHF calculations. The GC1 energy predicted by DFT (3794 cm^{-1}) is much lower than RHF (8813 cm^{-1}).[4] The DFT optimized N1-N15 and N15-H23 distance of GC1 (2.835 Å and 1.760 Å) are shorter than the RHF (2.840 Å and 1.793 Å). While Florian[4] uses different permittivity and cavity radius (ε = 40, a_0 = 5.0), the reaction field factor g [29] defined as $2(\varepsilon - 1)/((2\varepsilon + 1)\, a_0^3)$ of the present (8.5×10^{-3}) and Florian's calculation (7.7×10^{-3}) are very close, and cannot account for the difference. We therefore attribute this difference mainly to the level of calculation. Electron correlations stabilize the zwitterionic GC1 tautomer and the transition state GC‡01 connecting GC0 and GC1. Electron correlations are also known to decrease the transition barrier of proton transfer in malonaldehyde.[32]

From Table 2 we note that GC‡01(water) has shorter N7–O9 and N1–N15 distances and longer N7–H28 and N15–H23 bond lengths than those of GC0(water). This suggests that the first proton transfer (PT1) reaction is commenced by the guanine and cytosine moving closer to each other, as suggested by IRC calculation at the RHF level.[4]

2.2 A·T Base Pair

Geometry optimization of A·T tautomers was performed in the gas phase and in water. The cavity radius of AT0 (5.09 Å) calculated for the SCRF was used for the geometry optimization and normal mode calculations of AT0 and AT2. Two energy minima, AT0 and AT1 (Fig. 3), were found. AT0 is the most stable tautomer, and AT2 is produced by double proton transfer from AT0. The zwitterionic structure produced by single proton transfer from AT0 is not stable. The transition state between AT0 and AT2 (denoted AT‡02) was optimized as well. AT2 was not stable in the gas phase calculation. The relative energies of AT0, AT2, and AT‡02 are given in Table 3. The AT2 energy is 4737 cm^{-1}, and the transition state AT‡02 energy is slightly higher (4766 cm^{-1}). The small energy difference (29 cm^{-1}) indicates that the potential around the minimum of AT2 is very shallow. Calculated hydrogen bond geometries of all A·T tautomers are compared in Table 4.

Table 1. Relative energies of the stationary points (s.p.) of the base pair. The RHF calculations are from ref 4

tautomer	B3LYP/6-31G(d)		RHF/6-31G(d)
	ΔE (gas phase) (cm^{-1})	ΔE (in water) (cm^{-1})	ΔE (in water) (cm^{-1})
GC0	0	0	0
GC1	not s.p.	3794	8813
GC2	3761	3423	3896
GC‡01	–	3924	9583

Table 2. Calculated geometry of hydrogen bonds (Å) of G·C tautomers in water. Values in parenthesis are the bond lengths in the gas phase. Atom labels are shown in Fig. 4

bond	GC0	GC1	GC2	GC‡01
N7–H28	1.028 (1.037)	1.063	1.680 (1.728)	1.054
O9–H28	1.878 (1.775)	1.628	1.026 (1.009)	1.613
N7–O9	2.905 (2.812)	2.690	2.699 (2.731)	2.666
N15–H23	1.040 (1.034)	1.760	1.867 (1.849)	1.431
N1–H23	1.886 (1.905)	1.075	1.040 (1.049)	1.237
N1–N15	2.926 (2.944)	2.835	2.905 (2.897)	2.668
N19–H25	1.031 (1.023)	1.017	1.020 (1.016)	1.021
O8–H25	1.795 (1.095)	1.909	1.929 (1.961)	1.771
N19–O8	2.826 (2.938)	2.925	2.949 (2.977)	2.790

Table 3. Relative energies of the stationary points (s.p.) of the A·T base pair

structure	ΔE (gas phase) (cm^{-1})	ΔE (in water) (cm^{-1})
AT0	0	0
AT2	not s.p.	4737
AT‡02	–	4766

Table 4. Calculated geometry of hydrogen bonds (Å) of A·T tautomers in water. Values in parenthesis are the bond lengths in the gas phase. Atom labels are shown in Fig. 4

bond	AT0	AT2	AT‡02
N16–H26	1.846 (1.831)	1.048	1.055
N4–H26	1.043 (1.045)	1.750	1.714
N4–N16	2.889 (2.877)	2.791	2.762
O8–H21	1.905 (1.925)	1.071	1.138
N10–H21	1.023 (1.022)	1.511	1.381
N10–O8	2.926 (2.944)	2.581	2.518

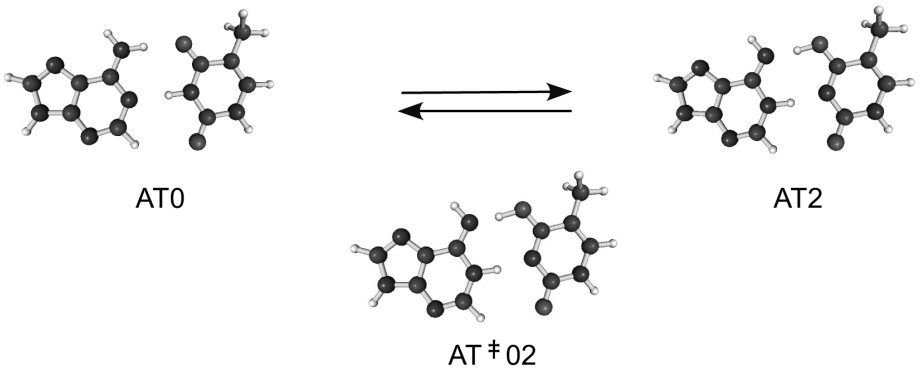

Fig. 3. Located energy minima of adenine·thymine base pair. Geometry optimizations were carried out at the B3LYP/6-31G(d,p) level with SCRF method assuming the cavity radius of 5.09 Å and the dielectric constant of 78.39 (water).

The optimized structure of AT‡02 is similar to AT2 (Fig. 3). However, as seen in Table 4, the N16–H26 and O8–H21 distances of AT‡02 are slightly longer than those of AT2, and N4–N16 and N10–O8 distances are slightly shorter than that of AT2, suggesting that the guanine and cytosine are closer and that the double proton transfer is not complete at AT‡02.

3. NORMAL MODE CALCULATIONS

3.1 G·C Base Pair

Normal modes were computed for the GC0, GC1, and GC2 tautomers. All frequencies of GC0 are real, but GC1 and GC2 have one out-of plane imaginary frequency (–57.0 and –3.4 respectively), indicating that G1 and GC2 are nonplanar. The previous study[4] suggests that there are no significant differences in energies and hydrogen bond lengths between the planar and nonplanar forms of GC1 and GC2.

The calculated normal modes with strong IR intensities are summarized in Tables 5, 6, and 7, and the atom labels are defined in Fig. 4. The carbonyl, N–H and O–H stretches have strong IR intensities and are most different among the three tautomers. The two carbonyl stretches of GC0 are located in the same frequency region (1753 and 1769 cm^{-1}), but the C10=O9 stretch of GC1 is at a lower frequency (1632), which may be attributed to the decrease of bond order with proton transfer (PT1). GC2 has no C10=O9 stretch peak in that region because the bonding becomes single.

Three N–H stretches of GC0 which are coupled to intermolecular hydrogen bondings have intense IR peaks at 3089 to 3326 cm^{-1}. The N1–H23 stretch of GC1 produced by the proton transfer (PT1) has the lowest frequency (2505 cm^{-1}) among the three N–H stretches, suggesting that this bond is very weak and unstable. The higher frequency (3090) of the N1–H23 stretch of GC2

Table 5. Linear infrared spectrum of GC0

mode no.	frequency (cm^{-1})	intensity	symmetry	assignment
68	1715.0	1429	A′	bend N19–H24, N19–H25, N7–H28, N7–H29
70	1753.6	64	A′	stretch C10–O9, C6–O8
71	1769.2	1608	A′	stretch C10–O9, C6–O8
72	3089.1	2267	A′	stretch N15–H23
76	3260.5	2732	A′	stretch N19–H25
77	3326.2	2666	A′	stretch N7–H28

Table 6. Linear infrared spectrum of GC1

mode no.	frequency (cm^{-1})	intensity	symmetry	assignment
65	1632.1	1852	A′	stretch C10–O9
71	1824.5	851	A′	stretch C6–O8
72	2504.8	3647	A′	stretch N1–H23
73	2721.2	7721	A′	stretch N7–H28
77	3496.2	1396	A′	stretch N19–H25

Table 7. Linear infrared spectrum of GC2

mode no.	frequency (cm^{-1})	intensity	symmetry	assignment
69	1703.6	956	A′	bend N19–H25, N19–H24
71	1803.2	988	A′	stretch C6–O8
72	2703.1	5612	A′	stretch O9–H28
73	3090.3	3576	A′	stretch N1–H23
77	3449.3	1667	A′	stretch N19–H25

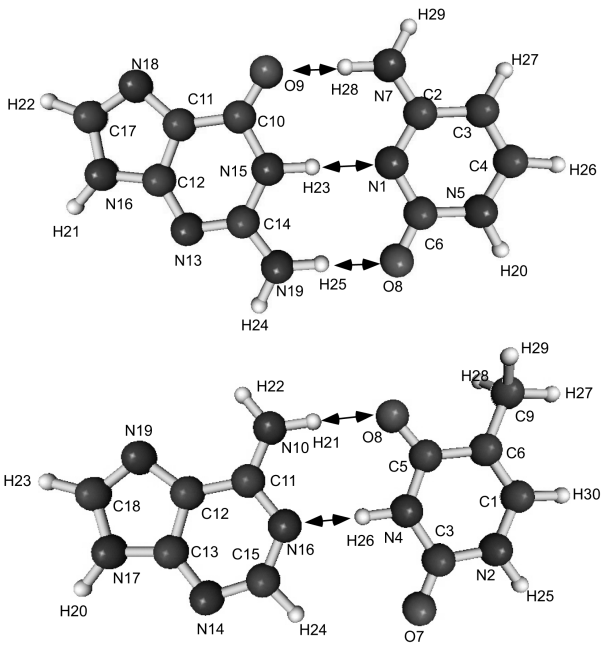

Fig. 4. Atom labels of GC0 and AT0 tautomers. Hydrogen bondings are indicated with double-headed arrows.

indicates stabilization by the second proton transfer (PT2). The O–H stretch of GC2 also shows a red-shifted peak at 2703 cm^{-1}, indicating a weak O9–H28 bonding.

Infrared experiments of DNA are sometimes carried out in D_2O to avoid masking the carbonyl stretch peaks by water. We have therefore calculated the normal modes of tautomers where the H20, 21, 23, 24, 25, 28, and 29 are deuterated (Tables 7, 9, and 10). The carbonyl stretch peaks of GC0 at 1735 and 1743 cm^{-1}, are red-shifted by ~20 cm^{-1} from the normal species. The N–H stretch modes of deuterated GC0 (2282–2428 cm^{-1}) are 800–900 cm^{-1} lower than the normal species. However, the characteristic changes of peak positions and intensities of deuterated species are similar to the normal species. The weak N–H stretch and O–H stretch peaks of GC1 and GC2 are found at 1900–2539 cm^{-1}.

3.2 A·T Base Pair

The above calculations were repeated for the AT0 and AT2 tautomers. All frequencies were found to be real, indicating stable ground states. Tables 11 and 12 show the normal modes with strong IR intensities. Infrared spectra have clear signatures of the geometry changes.

The carbonyl(C5–O8) stretch peak (1746 cm^{-1}) of AT0 is absent in AT2, and the strong O8–H21 stretch peak (1983 cm^{-1}) appears, because the AT0 carbonyl changes to hydroxyl in AT2 by protonation. The N4–

Table 8. Linear infrared spectrum of deuterated GC0

mode no.	frequency (cm^{-1})	intensity	symmetry	assignment
68	1619.3	1278	A′	stretch C14–N19
69	1688.3	655	A′	def(cytosine), stretch C3–C4
70	1735.1	1285	A′	stretch C6–O8
71	1743.4	1008	A′	stretch C10–O9
72	2281.7	1229	A′	stretch N15–H23
73	2387.1	1568	A′	stretch N19–H25
74	2428.4	1344	A′	stretch N7–H28

Table 9. Linear infrared spectrum of deuterated GC1

mode no.	frequency (cm^{-1})	intensity	symmetry	assignment
68	1624.5	1621	A′	stretch C10–O9, C2–N7
70	1680.9	1040	A′	stretch C2–N7, C10–O9
71	1785.6	634	A′	stretch C6–O8
72	1900.2	2287	A′	stretch N1–H23
73	2035.1	3600	A′	stretch N7–H28
77	2538.7	728	A′	stretch N19–H25

Table 10. Linear infrared spectrum of deuterated GC2

mode no.	frequency (cm^{-1})	intensity	symmetry	assignment
67	1613.3	1105	A′	def(guanine), stretch C2–N7
70	1679.8	1594	A′	def(cytosine), stretch C2–N7
71	1778.3	864	A′	stretch C6–O8
72	1994.5	2653	A′	stretch O9–H28
73	2282.7	1892	A′	stretch N1–H23
77	2509.6	895	A′	stretch N19–H25

Table 11. Linear infrared spectrum of AT0

mode no.	frequency (cm^{-1})	intensity	symmetry	assignment
69	1645.8	538	A′	def(adenine), stretch C11–C12, bend N10–H21
70	1704.0	625	A′	bend N10–H21, N10–H22
72	1745.9	745	A′	stretch C5–O8
73	1826.2	828	A′	stretch C3–O7
75	3069.1	3177	A′	stretch N4–H26
81	3380.7	2067	A′	stretch N10–H21

Table 12. Linear infrared spectrum of AT2

mode no.	frequency (cm^{-1})	intensity	symmetry	assignment
71	1675.8	1726	A′	bend O8–H21, stretch C1–C6
72	1733.5	712	A′	bend N16–H26, stretch C11–N10
73	1790.2	1168	A′	stretch C3–O7
74	1983.4	5356	A′	stretch O8–H21
75	2950.0	4980	A′	stretch N16–H26

Table 13. Linear infrared spectrum of deuterated AT0

mode no.	frequency (cm^{-1})	intensity	symmetry	assignment
70	1659.1	774	A′	def(adenine)
72	1723.1	993	A′	stretch C5–O8
73	1807.0	712	A′	stretch C3–O7
74	2265.9	1848	A′	stretch N4–H26
75	2462.4	1084	A′	stretch N10–H21

Table 14. Linear infrared spectrum of deuterated AT2

mode no.	frequency (cm^{-1})	intensity	symmetry	assignment
69	1571.5	940	A′	def(adenine)
72	1715.3	523	A′	def(thymine), stretch C11–N10, C1–C6
73	1725.3	132	A′	stretch O8–H21, C11–N10
74	1776.8	927	A′	stretch C3–O7
75	2185.8	2575	A′	stretch N16–H26

H26 stretch (3069) of AT0 is absent in the AT2 spectrum, and the N16–H26 stretch peak appears instead due to the double proton transfer. The N16–H26 stretch peak of AT2 (2950 cm^{-1}) is 119 cm^{-1} lower than the N4–H26 stretch peak of AT0 (3069 cm^{-1}), indicating that the N16–H26 bonding is weaker than N4–H26 bonding.

The normal mode calculations were repeated for the tautomers where the H21, 22, 25, and 26 are deuterated (Tables 13 and 14). The carbonyl stretches of AT0 at 1723 and 1807 cm^{-1}, are red-shifted by ~20 cm^{-1} from the normal species. The two N–H stretch modes of deuterated AT0 (2266 and 2462 cm^{-1}) are 803 and 918 lower than the normal species. The O–H stretch of deuterated AT2 is also red-shifted to 1725 cm^{-1} and coupled to C11-N10 stretch resulting in a weaker IR intensity.

4. CONCLUSIONS

We report all stable tautomers of guanine·cytosine (G·C) and adenine·thymine (A·T) Watson–Crick base pairs produced by single and double proton transfers from the most stable structures optimized using DFT at the B3LYP/6-31G(d,p) level. Calculations were performed both in the gas phase and in a medium with high dielectric constant (water: ε_r = 78.39) incorporated through the SCRF method. The cavity radii (G·C: 4.87 Å and A·T: 5.09 Å) were obtained at the most stable structures (GC0 and AT0) self-consistently by molecular volume calculations. In the gas phase, the zwitterionic tautomer of G·C base pair (GC1) is found to be unstable. However GC1 is stabilized in the high dielectric medium (water). AT2 is also unstable in the gas phase, but is stabilized in water. The relative stability of the tautomers and the proton transfer dynamics should be very sensitive to the surrounding environment. This can be related to the mechanism of the DNA replication.

The energy difference between AT2 and the transition state $AT^{\ddagger}02$ in water is very small (29 cm^{-1}), which indicates a shallow potential surface around the minimum of AT2. The DFT GC1 energy (3794 cm^{-1}) is much lower than the RHF level (8813 cm^{-1}).[4] Our study suggests that GC1 as well as GC2 can contribute to the nonlinear infrared spectra in the N–H stretch region, since these energies are much lower than the second harmonics of the N–H stretching modes, and these vibrational states can therefore be delocalized over the GC0, GC1 and GC2 tautomers.

Normal mode calculations performed for all stable G·C and A·T tautomers show that the characteristic changes of peak positions and intensities were similar for the normal and the deuterated species. Carbonyl and N–H (or O–H) stretch frequencies were most sensitive to the geometry differences both of G·C and A·T tautomers. The carbonyl stretch peaks (C10–O9 of GC0 and C5–O8 of AT0) are absent in the spectra of GC2 and AT2 because of the carbonyl protonation. The O–H stretches of GC2 and AT2 produced by the protonation have a very low frequency, suggesting weak bonding. The N–H stretch modes of unstable tautomers (GC1, GC2, and AT2) also have lower frequencies. The N1–H23 stretch mode of GC1 has the lowest frequency (normal: 2505 cm^{-1} and deuterated: 1900 cm^{-1}) among the three N–H stretch modes, indicating that the N1–H23 of GC1 is particularly weak and is stabilized in GC2 tautomer by the second proton transfer (PT2).

The energetics and the vibrational properties of the stable tautomers reported here constitute the first step for constructing an anharmonic vibrational exciton Hamiltonian[17,18,33] and simulating the nonlinear infrared spectra of the DNA.

Acknowledgments. We gratefully acknowledge the support of the National Institutes of Health (RO1 GM59230-03).

REFERENCES AND NOTES

(1) Saenger, W. *Principles of Nucleic Acid Structures;* Springer: Berlin, 1984.
(2) Jeffrey, G.; Saenger, W. *Hydrogen Bonding in Biological Structures;* Springer: Berlin, 1991.
(3) Lowdin, P.O. *Rev. Mod. Phys.* **1963**, *35*, 724–732.
(4) Florian, J.; Leszczynski, J. *J. Am. Chem. Soc.* **1996**, *118*, 3010–3017.
(5) Shukla, M. K.; Leszczynski, J. *J. Phys. Chem. A* **2002**, *106*, 11338–11346.
(6) Madsen, D.; Stenger, J.; Dreyer, J.; Nibbering, E.T.J.; Hamm, P.; Elsaesser, T. *Chem. Phys. Lett.* **2001**, *341*, 56–62.
(7) Thompson, W.H.; Hynes, J.T. *J. Phys. Chem. A* **2001**, *105*, 2582–2590.
(8) (a) Bixon, M.; Jortner, J. *J. Am. Chem. Soc.* **2001**, *123*, 12556–12567. (b) Jortner, J.; Bixon, M.; Voityuk, A. A.; Rosch, N. *J. Phys. Chem. A* **2002**, *106*, 7599–7606.
(9) Catalan, J.; Kasha, M. *J. Phys. Chem. A* **2000**, *104*, 10812–10820.
(10) Catalan, J.; Perez, P.; del Valle, J.C.; de Paz, J.L.G.; Kasha, M. *Proc. Natl. Acad. Sci. U.S.A.* **2002**, *99*, 5799–5803.
(11) Takeuchi, S.; Tahara, T. *J. Phys. Chem. A* **1998**, *102*, 7740–7753.
(12) Folmer, D.E.; Wisniewski, E.S.; Stairs, J.R.; Castleman, A.W. *J. Phys. Chem. A* **2000**, *104*, 10545–10549.
(13) T. Fiebig; Chachisvilis, M.; Manger, M.; Zewail, A.H.; Douhal, A.; Garcia-Ochoa, I.; Ayuso, A.D.H. *J. Phys. Chem. A* **1999**, *103*, 7419–7431.
(14) Ishikawa, H.; Iwata, K.; Hamaguchi, H. *J. Phys. Chem. A* **2002**, *106*, 2305–2312.
(15) Tsuboi, M. *Application of Infrared Spectrosocpy to Structure Studies of Nucleic Acids*. Vol. 3 of *Applied Spectroscopy Reviews*; Dekker: New York, 1969.
(16) Liquier, J.; Taillandier, E. In *Infrared Spectroscopy of Nucleic Acids*; *Infrared Spectroscopy of Biomolecules*; Mantsch, H.H.; Chapman, D., Eds.; Wiley-Liss, Inc: New York, 1996.
(17) Hayashi, T.; Mukamel, S. *Bull. Korean Chem. Soc.* **2003**, *24*, 1097–1101.
(18) Hayashi, T.; Mukamel, S. *J. Phys. Chem. A* **2003**, *107*, 9113–9131.
(19) Mukamel, S.; Hochstrasser, R.M. Special issue, *Chem. Phys.* **2001**, *135*.
(20) Mukamel, S. *Annu. Rev. Phys.* **2000**, *51*, 691–729.
(21) Demirdoven, N,; Khalil, M.; Golonzka, O.; Tokmakoff, A. *J. Phys. Chem. A* **2001**, *105*, 8025–8030.
(22) Golonzka, O.; Khalil, M.; Demirdoven, N,; Tokmakoff, A. *J. Chem. Phys.* **2001**, *115*, 10814–10828.
(23) Rector, K.D.; Zimdars, D.; Fayer, M.D. *J. Chem. Phys.* **1998**, *109*, 5455–5465.
(24) Wright, J.C.; Chen, P.C.; Hamilton, J.P.; Zilian, A.; Labuda, M.J. *Appl. Spectrosc.* **1997**, *51*, 949–958.
(25) Krummel, A.T.; Mukherjee, P.; Zanni, M.T. *J. Phys. Chem. B* **2003**, *107*, 9165–9169.
(26) GAUSSIAN 98 (Revision A.11). Frisch, M.J. et al. Gaussian, Inc., Pittsburgh, PA, 1998.
(27) Onsager, L. *J. Am. Chem. Soc.* **1936**, *58*, 1486.
(28) Wong, M.W.; Wiberg, K.B.; Frisch, M. *J. Chem. Phys.* **1991**, *95*, 8991–8998.
(29) Kirkwood, J.G. *J. Chem. Phys.* **1934**, *2*, 713.
(30) Wong, M.W.; Frisch, M. J.; Wiberg, K. B. *J. Am. Chem. Soc.* **1991**, *113*, 4776–4782.
(31) Wiberg, K.B.; Wong, M.W. *J. Am. Chem. Soc.* **1993**, *115*, 1078–1804.
(32) Benderskii, V.A.; Vetoshkin, E.V.; Irgibaeva, I.S.; Trommsdorff, H.-P. *Russ. Chem. Bull.* **2001**, *50*, 1148–1158.
(33) Moran, A.M.; Park, S.-M.; Dreyer, J.; Mukamel, S. *J. Chem. Phys.* **2003**, *118*, 3651–3659.